

A lowest-order locking-free conforming virtual element method based on the reduced integration technique for linear elasticity problems

Jianguo Huang^{a,*}, Sen Lin^a, Yue Yu^{a,b}

^a*School of Mathematical Sciences, and MOE-LSC, Shanghai Jiao Tong University, Shanghai 200240, China*

^b*Institute of Natural Sciences, Shanghai Jiao Tong University, Shanghai 200240, China*

Abstract

This paper develops a lowest-order conforming virtual element method for planar linear elasticity in the displacement/traction formulation, which can be viewed as an extension of the idea in Brenner & Sung (1992) to the virtual element method, with the family of polygonal meshes satisfying a very general geometric assumption. The method is shown to be uniformly convergent with the Lamé constant with the optimal rates of convergence.

Keywords: Virtual element method, Linear elasticity, Locking-free, Reduced integration technique.

1. Introduction

The linear elastic model is of fundamental importance in elasticity. The construction and analysis of its numerical algorithms can help to solve or analyze more complex engineering problems. In linear elasticity, the Lamé constant λ is an important parameter, which characterizes the compressibility of the material. For small λ , this problem can be treated as the Poisson equation in vector form. However, when λ tends to infinity or the material is nearly incompressible, it becomes very difficult to design low order finite element methods (FEMs) with parameter-free or locking-free convergence. For this reason, several methods or techniques have been developed in the literature to tackle with this problem. One can refer to [12, 22, 24] and the references therein for details.

The virtual element method (VEM) is a newly proposed numerical method in recent years as a generalization of the finite element method on polygonal or polyhedral meshes (cf. [2, 5, 7]). Compared with the FEM, it may be much easier to construct a locking-free virtual element due to the flexibility of the construction of the virtual element spaces. The conforming VEMs for the linear elasticity problem are first proposed in [6], where a locking-free analysis is also carried out. However, the order $k \geq 2$ is required to ensure the so-called discrete inf-sup condition and the optimal convergence order in the H^1 norm, which is consistent with the classical conforming FEM. In [28], a low-order locking-free virtual element space is constructed for the linear elasticity problems, which can be seen as an evolution of the Bernardi-Raugel finite element to general polygonal meshes. The a priori estimates are shown to be optimal and uniform with respect to the Lamé constant, which is achieved by adding extra degrees of freedom so that the inf-sup condition can be satisfied easily. Nonconforming VEMs for the linear elasticity problems are first introduced in [30] for the pure displacement formulation both in two and three dimensions, and the pure traction formulation in two dimensions. The nonconforming VEM is uniformly convergent for $k \geq 2$ under some hypotheses, which, however, may be unstable for $k = 1$. Some other VEMs for elasticity problems in two and three dimensions can be found in [3, 4, 8, 10, 14, 19, 20, 21, 23, 25, 26, 29].

In this paper, we are intended to generalize the idea in [12] to construct a lowest-order conforming locking-free VEM for solving the linear elasticity problems. In the literature of VEMs, the local bilinear form $(\operatorname{div} \mathbf{v}, \operatorname{div} \mathbf{w})_E$ of the continuous variational problem is usually approximated by $(\Pi_0^E \operatorname{div} \mathbf{v}, \Pi_0^E \operatorname{div} \mathbf{w})_E$, where E is a polygon and Π_0^E is the L^2 projection. The above treatment is proved to be locking-free only for $k \geq 2$ in [6]. Different from the remedy in [28] by introducing some additional moments, we first refine the initial mesh in some way and establish the VEM on the resulting fine mesh as in the classical treatment; then we replace the L^2 projection Π_0^E by the one on the coarse mesh, denoted by Π_0^K , where E and K are generic elements in the fine mesh and coarse mesh, respectively, satisfying $E \subset K$. This technique is referred to as the reduced integration technique (cf. [22, 24, 12]), which is shown to be effective and parameter-free for the virtual element methods as observed in this article.

*Corresponding author

Email addresses: jghuang@sjtu.edu.cn (Jianguo Huang), sjtu_Einsteinlin7@sjtu.edu.cn (Sen Lin), terenceyuyue@sjtu.edu.cn (Yue Yu)

We end this section by introducing some notations. We use standard notation for Sobolev spaces and norms (see [1] for more details). Let D be any open subset of Ω and $|D|$ denote the area of D . Given a non-negative integer s , we denote the standard Sobolev spaces on D by $H^s(D)$ with norm $\|\cdot\|_{s,D}$ and semi-norm $|\cdot|_{s,D}$, and denote the L^2 -inner product on D by $(\cdot, \cdot)_D$. By convention, $H^0(D) = L^2(D)$. Let $\mathbb{P}_s(D)$ be the set of polynomials of degree less than s on D . Moreover, we omit the subscript when $D = \Omega$. For the vector-valued functions or spaces, we use the bold symbols, such as \mathbf{v} , $L^2(\Omega)$, $\mathbf{H}^s(\Omega)$, $\mathbf{H}_0^s(\Omega)$, etc. For any two quantities a and b , “ $a \lesssim b$ ” indicates “ $a \leq Cb$ ” with the hidden generic positive constant C independent of the Lamé constant λ and the mesh size, which may take different values at different occurrences, and $a \approx b$ shows $a \lesssim b \lesssim a$.

2. The linear elasticity problem

Let $\Omega \subset \mathbb{R}^2$ be a bounded polygonal domain with the boundary $\partial\Omega$. Given a body force \mathbf{f} defined on Ω , the linear elasticity problem is to find the displacement vector $\mathbf{u} = (u_1, u_2)^\top$ that solves

$$\begin{cases} -\operatorname{div} \boldsymbol{\sigma}(\mathbf{u}) = \mathbf{f} & \text{in } \Omega, \\ \mathbf{u} = \mathbf{0} & \text{on } \partial\Omega, \end{cases} \quad (2.1)$$

where $\operatorname{div} \mathbf{u} = \partial_1 u_1 + \partial_2 u_2$. The constitutive relation for the linear elasticity is

$$\boldsymbol{\sigma} = 2\mu \boldsymbol{\varepsilon}(\mathbf{u}) + \lambda(\operatorname{div} \mathbf{u})\mathbf{I},$$

where $\boldsymbol{\sigma} = (\sigma_{ij})$ and $\boldsymbol{\varepsilon} = (\varepsilon_{ij})$ are the second order stress and strain tensors, respectively, satisfying $\varepsilon_{ij} = \frac{1}{2}(\partial_i u_j + \partial_j u_i)$, λ and μ are the Lamé constants satisfying $\mu \in [\mu_1, \mu_2]$ with $0 < \mu_1 < \mu_2$ and $\lambda \in (0, \infty)$, and \mathbf{I} is the identity matrix. We recall that the following Korn's inequality holds (cf. [11]):

$$\|\mathbf{v}\|_1 \lesssim \|\boldsymbol{\varepsilon}(\mathbf{v})\|_0, \quad \mathbf{v} \in \mathbf{H}_0^1(\Omega). \quad (2.2)$$

Given $\mathbf{f} \in L^2(\Omega)$, the variational formulation of (2.1) is to find $\mathbf{u} \in \mathbf{V} = \mathbf{H}_0^1(\Omega)$ such that

$$a(\mathbf{u}, \mathbf{v}) = (\mathbf{f}, \mathbf{v}), \quad \mathbf{v} \in \mathbf{V}, \quad (2.3)$$

where

$$a(\mathbf{w}, \mathbf{v}) = 2\mu(\boldsymbol{\varepsilon}(\mathbf{w}), \boldsymbol{\varepsilon}(\mathbf{v})) + \lambda(\operatorname{div} \mathbf{w}, \operatorname{div} \mathbf{v}), \quad \mathbf{w}, \mathbf{v} \in \mathbf{V}, \quad (2.4)$$

and

$$(\mathbf{f}, \mathbf{v}) = \int_{\Omega} \mathbf{f} \mathbf{v} \, dx, \quad \mathbf{v} \in \mathbf{V}.$$

By the Korn's inequality (2.2), it is easy to obtain the boundedness and coercivity of $a(\cdot, \cdot)$:

$$\begin{aligned} a(\mathbf{w}, \mathbf{v}) &\lesssim (1 + \lambda)|\mathbf{w}|_1|\mathbf{v}|_1, \quad \mathbf{w}, \mathbf{v} \in \mathbf{V}, \\ |\mathbf{v}|_1^2 &\lesssim a(\mathbf{v}, \mathbf{v}), \quad \mathbf{v} \in \mathbf{V}, \end{aligned}$$

which imply that the problem (2.1) has a unique solution by the Lax-Milgram lemma (cf. [11]). For ease of presentation, we define

$$a_{\mu}(\mathbf{w}, \mathbf{v}) = (\boldsymbol{\varepsilon}(\mathbf{w}), \boldsymbol{\varepsilon}(\mathbf{v})).$$

It is also well known that there holds the regularity estimate

$$\|\mathbf{u}\|_2 + \lambda\|\operatorname{div} \mathbf{u}\|_1 \lesssim \|\mathbf{f}\|_0, \quad (2.5)$$

when Ω is a convex polygonal domain, see [12] for example.

3. Virtual element methods for the pure displacement problem

In this section, we propose a locking-free conforming virtual element method by using the reduced integration technique. This is the generalization of the locking-free finite element method introduced in [12] to the context of the virtual element methods.

3.1. Mesh assumption and the virtual element space

Let $\{\mathcal{T}_h\}$ be a family of decompositions of Ω into polygonal elements. The generic element is denoted by K with diameter $h_K = \text{diam}(K)$. For clarity of presentation, we first work on meshes satisfying a stronger mesh assumption than the one given in [13, 16]:

C0. For each element K , there exist positive constant γ_1, γ_2 independent of h_K such that (cf. [5])

- K is star-shaped with respect to a disc in K with radius $\geq \gamma_1 h_K$;
- the distance between any two vertices of K is $\geq \gamma_2 h_K$.

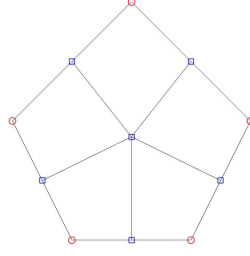


Fig. 1: The first type of mesh refinement. The refined element satisfying the mesh assumption **C0**. The small quadrilateral element of the fine mesh and the large polygonal element of the original mesh are denoted by E and K , respectively.

Under the above assumption, one easily finds that the mesh can be refined by connecting the barycenter of the disc with the midpoints of the edges of K as depicted in Fig. 1. The resulting finer meshes will be denoted by \mathcal{T}_h^* with generic element given by E . Here, $h = \max_{E \in \mathcal{T}_h^*} h_E$.

In this paper, we consider the lowest-order conforming virtual element space (VES) defined on the finer mesh \mathcal{T}_h^* . To this end, we briefly review the construction proposed in [5]. The local scalar virtual element space on E is defined as

$$V_1(E) = \{v \in H^1(E) \mid \Delta v = 0 \text{ on } E, v|_e \in \mathbb{P}_1(e), \quad e \subset \partial E\}. \quad (3.1)$$

The corresponding degrees of freedoms (DOFs) are:

- $\chi_i \in \chi$: the value at vertices of E ,

$$\chi_i(v) = v(z_i), \quad z_i \text{ is the vertex of } E.$$

The local virtual element space for linear elasticity is then given by the tensor product space $\mathbf{V}_1(E) = (V_1(E))^2$.

In what follows, denote by \mathbf{V}_h the global VES, which is defined elementwise and required that the degrees of freedom are continuous through the interior vertices while zero for the boundary DOFs, i.e.,

$$\mathbf{V}_h = \{\mathbf{v} \in \mathbf{H}_0^1(\Omega) \mid \mathbf{v}|_E \in \mathbf{V}_1(E), \quad E \in \mathcal{T}_h^*\}.$$

3.2. The virtual element method based on the reduced integration technique

As in [6, 30], we first introduce the elliptic projection $\Pi_1^E: \mathbf{H}^1(E) \rightarrow (\mathbb{P}_1(E))^2$ for the first term of (2.4), which satisfies

$$\begin{cases} (\boldsymbol{\varepsilon}(\Pi_1^E \mathbf{v}), \boldsymbol{\varepsilon}(\mathbf{p}))_E = (\boldsymbol{\varepsilon}(\mathbf{v}), \boldsymbol{\varepsilon}(\mathbf{p}))_E, & \mathbf{p} \in (\mathbb{P}_1(E))^2, \\ \int_{\partial E} \Pi_1^E \mathbf{v} \, ds = \int_{\partial E} \mathbf{v} \, ds, \\ \int_E \text{rot } \Pi_1^E \mathbf{v} \, dx = \int_E \text{rot } \mathbf{v} \, dx, \end{cases} \quad (3.2)$$

where $\text{rot } \mathbf{v} = \partial_1 v_2 - \partial_2 v_1$. One can check that the elliptic projection Π_1^E can be computed by the given DOFs. For simplicity, we write Π_1 for the related elementwise defined global operator.

For the second term of (2.4), a common practice is to introduce the L^2 projection $\Pi_{k-1}^0 \text{div}$ on E . However, the theoretical analysis in [6] ensures the locking-free property only for $k \geq 2$. For this reason, the authors in [28] add extra degrees of freedom related to the normal component of \mathbf{v} on each edge, and hence introduce a Bernardi-Raugel type virtual element for polygonal meshes.

We now consider a different approach that is used in [12] for the scenario of finite element methods. The main idea is to define the L^2 projection $\Pi_{k-1}^0 \operatorname{div}$ on the element K of the coarse mesh \mathcal{T}_h instead of the element E of the fine mesh \mathcal{T}_h^* , where $k = 1$. To avoid confusion, we denote the new L^2 projection by $\Pi_0^K \operatorname{div}$, defined as follows:

$$\begin{cases} \Pi_0^K \operatorname{div} : V_1(K) \rightarrow \mathbb{P}_0(K), & \mathbf{v} \mapsto \Pi_0^K \operatorname{div} \mathbf{v}, \\ \int_K (\Pi_0^K \operatorname{div} \mathbf{v}) p \, dx = \int_K (\operatorname{div} \mathbf{v}) p \, dx, & p \in \mathbb{P}_0(K), \end{cases} \quad (3.3)$$

where $V_1(K) = V_h|_K$. We also extend the definition of $\Pi_0^K \operatorname{div}$ to $\mathbf{H}^1(K)$. Noting that

$$\int_K \operatorname{div} \mathbf{v} \, dx = \int_{\partial K} \mathbf{v} \cdot \mathbf{n} \, ds,$$

we can compute $\Pi_0^K \operatorname{div} \mathbf{v}$ only using the values at the vertices of K for all $\mathbf{v} \in V_1(K)$.

With the help of the above projections, we are in a position to introduce the following local computable bilinear form

$$a_h^K(\mathbf{w}_h, \mathbf{v}_h) = 2\mu \sum_{E \subset K} a_{\mu,h}^E(\mathbf{w}_h, \mathbf{v}_h) + \lambda (\Pi_0^K \operatorname{div} \mathbf{w}_h, \Pi_0^K \operatorname{div} \mathbf{v}_h)_K, \quad \mathbf{w}_h, \mathbf{v}_h \in V_1(K), \quad (3.4)$$

where

$$a_{\mu,h}^E(\mathbf{w}_h, \mathbf{v}_h) = (\boldsymbol{\varepsilon}(\Pi_1^E \mathbf{w}_h), \boldsymbol{\varepsilon}(\Pi_1^E \mathbf{v}_h))_E + S^E(\mathbf{w}_h - \Pi_1^E \mathbf{w}_h, \mathbf{v}_h - \Pi_1^E \mathbf{v}_h)$$

and

$$S^E(\mathbf{w}_h, \mathbf{v}_h) = \boldsymbol{\chi}(\mathbf{w}_h) \cdot \boldsymbol{\chi}(\mathbf{v}_h) = \sum_{i=1}^{N_v} \chi_i(\mathbf{w}_h) \cdot \chi_i(\mathbf{v}_h)$$

with N_v being the number of the vertices of E .

The locking-free conforming VEM of the variational problem (2.3) is to find $\mathbf{u}_h \in V_h$ such that

$$a_h(\mathbf{u}_h, \mathbf{v}_h) = \langle \mathbf{f}_h, \mathbf{v}_h \rangle, \quad \mathbf{v}_h \in V_h, \quad (3.5)$$

where

$$a_h(\mathbf{u}_h, \mathbf{v}_h) = \sum_{K \in \mathcal{T}_h} a_h^K(\mathbf{u}_h, \mathbf{v}_h),$$

and the approximation of the right hand side is given by

$$\langle \mathbf{f}_h, \mathbf{v}_h \rangle = (\mathbf{f}, P_h \mathbf{v}_h), \quad (3.6)$$

where

$$P_h \mathbf{v}_h|_E = \frac{1}{N_v} \sum_{i=1}^{N_v} \mathbf{v}_h(z_i).$$

3.3. Stability of the virtual element method

To figure out the geometric dependence of the hidden constants, we first recall a classic Korn's inequality with respect to star-shaped domains.

Lemma 3.1 ([12, 18]). *Let $D \subset \mathbb{R}^2$ be a bounded domain of diameter h , which is star-shaped with respect to a disc of radius ρ . Then for any $\mathbf{v} \in \mathbf{H}^1(D)$ satisfying $\int_D \operatorname{rot} \mathbf{v} \, dx = 0$, there holds*

$$|\mathbf{v}|_{1,D} \lesssim \|\boldsymbol{\varepsilon}(\mathbf{v})\|_{0,D},$$

where the hidden constant C only depends on the aspect ratio h/ρ .

With the help of the above lemmas, we are able to derive the norm equivalence and the stability condition for the proposed virtual element method (3.5) described as follows.

Theorem 3.1. *Under the mesh assumption C0, for all $\mathbf{v}_h \in V_h$ there hold*

$$\|\boldsymbol{\varepsilon}(\mathbf{v}_h - \Pi_1^E \mathbf{v}_h)\|_{0,E} \approx \|\boldsymbol{\chi}(\mathbf{v}_h - \Pi_1^E \mathbf{v}_h)\|_{\rho}, \quad E \in \mathcal{T}_h^*, \quad (3.7)$$

and

$$a_{\mu,h}^E(\mathbf{v}_h, \mathbf{v}_h) \approx a_{\mu}^E(\mathbf{v}_h, \mathbf{v}_h), \quad E \in \mathcal{T}_h^*. \quad (3.8)$$

Proof. By definition of Π_1^E and Lemma 3.1, one has

$$\|\varepsilon(\mathbf{v}_h - \Pi_1^E \mathbf{v}_h)\|_{0,E} \approx |\mathbf{v}_h - \Pi_1^E \mathbf{v}_h|_{1,E}, \quad \mathbf{v}_h \in V_h. \quad (3.9)$$

According to the norm equivalence in [16], we have

$$h_K^{-1} \|\mathbf{v}\|_{0,E} \approx \|\chi(\mathbf{v})\|_2$$

for any $\mathbf{v} \in V_1(E)$, and hence

$$h_K^{-1} \|\mathbf{v}_h - \Pi_1^E \mathbf{v}_h\|_{0,E} \approx \|\chi(\mathbf{v}_h - \Pi_1^E \mathbf{v}_h)\|_2. \quad (3.10)$$

In view of the inverse inequality in [16] and the standard Poincaré-Friedrichs inequality, we further obtain

$$h_K^{-1} \|\mathbf{v}_h - \Pi_1^E \mathbf{v}_h\|_{0,E} \approx |\mathbf{v}_h - \Pi_1^E \mathbf{v}_h|_{1,E},$$

which together with (3.9) and (3.10) yields the first relation.

Since

$$a_\mu^E(\mathbf{v}_h, \mathbf{v}_h) = \|\varepsilon(\mathbf{v}_h)\|_{0,E}^2 = \|\varepsilon(\Pi_1^E \mathbf{v}_h)\|_{0,E}^2 + \|\varepsilon(\mathbf{v}_h - \Pi_1^E \mathbf{v}_h)\|_{0,E}^2,$$

the second relation follows from the first one. \square

4. Error analysis

Following the similar arguments in [6], we can derive an abstract lemma for error analysis.

Lemma 4.1. *Let $\mathbf{u} \in V$ and $\mathbf{u}_h \in V_h$ be the solution of the problem (2.3) and (3.5), respectively. Then under the mesh assumption C0, for any $\mathbf{u}_I \in V_h$ and for any piecewise polynomial $\mathbf{u}_\pi \in (\mathbb{P}_k(\mathcal{T}_h^*))^2$, there holds*

$$|\mathbf{u} - \mathbf{u}_h|_1 \lesssim (|\mathbf{u} - \mathbf{u}_I|_1 + |\mathbf{u} - \mathbf{u}_\pi|_{1,h} + \lambda \|\operatorname{div} \mathbf{u} - \Pi_0 \operatorname{div} \mathbf{u}_I\|_0 + \|\mathbf{f} - \mathbf{f}_h\|_{V_h'}), \quad (4.1)$$

where $\Pi_0 \operatorname{div} \mathbf{v}|_K = \Pi_0^K \operatorname{div} \mathbf{v}$ for all $\mathbf{v} \in V$, and

$$\|\mathbf{f} - \mathbf{f}_h\|_{V_h'} = \sup_{\mathbf{v} \in V_h} \frac{(\mathbf{f}, \mathbf{v}_h) - \langle \mathbf{f}_h, \mathbf{v}_h \rangle}{|\mathbf{v}_h|_1}. \quad (4.2)$$

Proof. By setting $\delta_h = \mathbf{u}_h - \mathbf{u}_I$ and using the triangle's inequality, it suffices to bound $|\delta_h|_1$. According to the equivalence (3.8) and the Korn's inequality (2.2), we have the coercivity

$$|\delta_h|_1^2 \lesssim \|\varepsilon(\delta_h)\|_0^2 = a_\mu(\delta_h, \delta_h) \approx a_{\mu,h}(\delta_h, \delta_h).$$

The following argument is standard, so we omit it for simplicity. One can refer to the proof of Theorem 3.2 in [6] for details. \square

We now prove the locking-free property of the proposed VEM. To this end, we shall introduce a special interpolation operator as presented in the proof of the following lemma.

Lemma 4.2. *Let $\mathbf{u} \in \mathbf{H}_0^1(\Omega) \cap \mathbf{H}^2(\Omega)$ be the solution of problem (2.3). Then there exists a VEM function $\mathbf{u}_I \in V_h$ such that*

$$\Pi_0^K \operatorname{div} \mathbf{u}_I = \Pi_0^K \operatorname{div} \mathbf{u}, \quad K \in \mathcal{T}_h, \quad (4.3)$$

and

$$|\mathbf{u} - \mathbf{u}_I|_1 \lesssim h|\mathbf{u}|_2. \quad (4.4)$$

Proof. By definition of $\Pi_0^K \operatorname{div}$ and by integration by parts, one has

$$\Pi_0^K \operatorname{div} \mathbf{u} = \int_K \operatorname{div} \mathbf{u} \, dx = \int_{\partial K} \mathbf{u} \cdot \mathbf{n} \, ds = \sum_{e \subset \partial K} \int_e \mathbf{u} \cdot \mathbf{n} \, ds,$$

thus the first relation (4.3) is equal to

$$\sum_{e \in \partial K} \int_e \mathbf{u}_I \cdot \mathbf{n} \, ds = \sum_{e \in \partial K} \int_e \mathbf{u} \cdot \mathbf{n} \, ds.$$

It suffices to construct a VEM function $\mathbf{u}_I \in \mathbf{V}_h$ such that

$$\int_e \mathbf{u}_I \, ds = \int_e \mathbf{u} \, ds, \quad e \subset \partial K.$$

We construct the function \mathbf{u}_I by determining its DOF values. For any edge e of K with two end points z_1 and z_2 , denote the middle point of e by z_0 . Then the edge e is divided into two subedges $e_1 = \overline{z_1 z_0}$ and $e_2 = \overline{z_0 z_2}$. For the endpoints, we let

$$\mathbf{u}_I(z_i) = \mathbf{u}(z_i), \quad i = 1, 2.$$

For the center z_c of the disc (see Fig. 1), we define

$$\mathbf{u}_I(z_c) = \mathbf{u}(z_c).$$

Since \mathbf{u}_I is piecewise linear along ∂K , we have

$$\begin{aligned} \int_e \mathbf{u} \, ds &= \int_e \mathbf{u}_I \, ds = \int_{e_1} \mathbf{u}_I \, ds + \int_{e_2} \mathbf{u}_I \, ds \\ &= \frac{|e_1|}{2} (\mathbf{u}_I(z_1) + \mathbf{u}_I(z_0)) + \frac{|e_2|}{2} (\mathbf{u}_I(z_0) + \mathbf{u}_I(z_2)) \\ &= \frac{|e|}{4} (\mathbf{u}_I(z_1) + \mathbf{u}_I(z_2) + 2\mathbf{u}_I(z_0)), \end{aligned}$$

which forces us to define

$$\mathbf{u}_I(z_0) = \frac{2}{|e|} \int_e \mathbf{u} \, ds - \frac{\mathbf{u}_I(z_1) + \mathbf{u}_I(z_2)}{2} = \frac{2}{|e|} \int_e \mathbf{u} \, ds - \frac{\mathbf{u}(z_1) + \mathbf{u}(z_2)}{2}.$$

The Assumption **C0** implies the existence of a globally shape-regular sub-triangulation $\widehat{\mathcal{T}}_h$ of \mathcal{T}_h . Then according to [17], for $\mathbf{u} \in \mathbf{H}_0^1(\Omega) \cap \mathbf{H}^s(\Omega)$ ($1 \leq s \leq k+1$), there exists a classical Cl  ment interpolant $\mathbf{u}_c \in (\mathbb{P}_k(\widehat{\mathcal{T}}_h)) \cap \mathbf{H}_0^1(\Omega)$ of \mathbf{u} such that

$$\|\mathbf{u} - \mathbf{u}_c\|_{0,T} + h\|\mathbf{u} - \mathbf{u}_c\|_{1,T} \leq \hat{C}_{Clem} h^s |\mathbf{u}|_{s,\widehat{T}}, \quad T \in \widehat{\mathcal{T}}_h. \quad (4.5)$$

Here, $\hat{C}_{Clem} > 0$ depends only on the polynomial degree k and on the mesh regularity. and \widehat{T} denotes the usual finite element patch relative to T . From the construction of $\mathbf{u}_I \in \mathbf{V}_1(K)$, we have $\mathbf{u}_I|_{\partial K} = \mathbf{u}_c|_{\partial K}$, then by [15] there holds:

$$\|\mathbf{u}_c - \mathbf{u}_I\|_{1,K} \leq C(\|\mathbf{u} - \mathbf{u}_c\|_{1,K} + \|\mathbf{u} - \Pi_0^K \mathbf{u}\|_{1,K}) \quad (4.6)$$

with C independent of h_K . Here $\Pi_0^K \mathbf{u}$ denotes the usual L^2 projection of \mathbf{u} onto $(\mathbb{P}_0(K))^2$. Combining with the triangle inequality, (4.5), (4.6) and the L^2 projection error estimates yields

$$\|\mathbf{u} - \mathbf{u}_I\|_{1,K} \leq \|\mathbf{u} - \mathbf{u}_c\|_{1,K} + \|\mathbf{u}_c - \mathbf{u}_I\|_{1,K} \leq Ch_K \|\mathbf{u}\|_{2,\omega(K)}, \quad (4.7)$$

where C independent of h_K and $\omega(K)$ denotes the patch consisting of the element K and its neighbours, which implies the second relation (4.4). \square

Combining Lemmas 4.1-4.2, the projection error estimates (cf. [11]) and the estimate for (4.2) (cf. [6]), we are able to derive the following error estimate which is uniform with the incompressible parameter λ .

Theorem 4.1. *Let \mathbf{u} and \mathbf{u}_h be given as in Lemma 4.1. Under the mesh assumption **C0** and the condition of regularity estimate (2.5), there holds*

$$\|\mathbf{u} - \mathbf{u}_h\|_1 \lesssim h \|\mathbf{f}\|_0, \quad (4.8)$$

with the hidden positive constant C independent of h and λ .

Using the duality argument and following the similar proof of Theorem 4.4 in [28], we can establish the error estimate in L^2 norm.

Theorem 4.2. *Assume that the domain Ω is convex. Under the same assumptions of Theorem 4.1, there holds*

$$\|\mathbf{u} - \mathbf{u}_h\|_0 \lesssim h^2 \|\mathbf{f}\|_0. \quad (4.9)$$

5. The VEM for the pure traction problem

In this section, we extend our approach to the pure traction problem described as follows:

$$\begin{cases} -\operatorname{div} \sigma(\mathbf{u}) = \mathbf{f} & \text{in } \Omega, \\ \sigma(\mathbf{u}) \mathbf{n} = \mathbf{0} & \text{on } \partial\Omega, \end{cases} \quad (5.1)$$

where \mathbf{n} denotes the exterior unit vector normal to $\partial\Omega$. The problem (5.1) is uniquely solvable in \mathbf{W} defined later if and only if \mathbf{f} satisfies the following compatibility condition (cf. [11, 12])

$$\int_{\Omega} \mathbf{f} \cdot \mathbf{v} \, dx = 0, \quad \mathbf{v} \in \mathbf{RM},$$

where

$$\mathbf{RM} = \{\mathbf{v} \mid \mathbf{v} = (a + bx_2, c - bx_1)^T, \, a, b, c \in \mathbb{R}\}.$$

We define the admissible space as (cf. [11])

$$\mathbf{W} = \left\{ \mathbf{v} \in \mathbf{H}^1(\Omega) \mid \int_{\Omega} \mathbf{v} \, dx = \mathbf{0}, \int_{\Omega} \operatorname{rot} \mathbf{v} \, dx = 0 \right\}.$$

The continuous variational problem (5.1) is the same as the one given in (2.3), with the function space replaced by \mathbf{W} . As was done in [2, 30], we introduce an enhancement virtual element space as

$$\mathbf{W}_1(E) = \{\mathbf{v} \in \mathbf{H}^1(E) \mid \Delta \mathbf{v} \in (\mathbb{P}_0(E))^2, (\mathbf{v}, \mathbf{1})_E = (\Pi_1^E \mathbf{v}, \mathbf{1})_E, \mathbf{v}|_e \in (\mathbb{P}_1(e))^2, \, e \subset \partial E\},$$

with the global VES given by

$$\mathbf{W}_h = \left\{ \mathbf{v}_h \in \mathbf{L}^2(\Omega) \mid \mathbf{v}_h|_E \in \mathbf{W}_1(E), \, E \in \mathcal{T}_h, \int_{\Omega} \mathbf{v}_h \, dx = \mathbf{0}, \int_{\Omega} \operatorname{rot} \mathbf{v}_h \, dx = 0 \right\}.$$

Let \mathbf{v}_I be the interpolation of $\mathbf{v} \in \mathbf{W}_h$. One can easily check that

$$\int_{\Omega} \mathbf{v}_I \, ds = \mathbf{0}, \quad \int_{\Omega} \operatorname{rot} \mathbf{v}_I \, dx = 0$$

by the integration by parts, which shows $\mathbf{v}_I \in \mathbf{W}_h$.

The locking-free conforming VEM of problem (5.1) is to find $\mathbf{u}_h \in \mathbf{W}_h$ such that

$$a_h(\mathbf{u}_h, \mathbf{v}_h) = \langle \mathbf{f}_h, \mathbf{v}_h \rangle, \quad \mathbf{v}_h \in \mathbf{W}_h. \quad (5.2)$$

Here, the construction of the computable bilinear form and the approximation of the right hand side are the same with that in (5.2).

We now establish a same result as in Lemma 4.2.

Lemma 5.1. *Let $\mathbf{u} \in \mathbf{H}_0^1(\Omega) \cap \mathbf{H}^2(\Omega)$ be the weak solution of problem (5.1). Then there exists a VEM function $\mathbf{u}_{\mathcal{G}} \in \mathbf{W}_h$ such that*

$$\Pi_0^K \operatorname{div} \mathbf{u}_{\mathcal{G}} = \Pi_0^K \operatorname{div} \mathbf{u}, \quad K \in \mathcal{T}_h,$$

and

$$|\mathbf{u} - \mathbf{u}_{\mathcal{G}}|_1 \lesssim h |\mathbf{u}|_2.$$

Proof. Let \mathbf{u}_I be the function given in Lemma 4.2. By the integration by parts, it immediately gives

$$\Pi_0^K \operatorname{div} \mathbf{u}_I = \Pi_0^K \operatorname{div} \mathbf{u}, \quad \Pi_0^K \operatorname{rot} \mathbf{u}_I = \Pi_0^K \operatorname{rot} \mathbf{u}, \quad K \in \mathcal{T}_h.$$

Define

$$\mathbf{u}_{\mathcal{G}} = \mathbf{u}_I - \frac{1}{|\Omega|} \int_{\Omega} \mathbf{u}_I \, dx.$$

We then have

$$\int_{\Omega} \mathbf{u}_{\mathcal{G}} \, dx = \mathbf{0}, \quad \int_{\Omega} \operatorname{rot} \mathbf{u}_{\mathcal{G}} \, dx = 0,$$

which indicates $\mathbf{u}_{\mathcal{G}} \in \mathbf{W}_h$. The estimates obviously follows from (4.4). □

With the help of the above lemma and following the same argument in Section 4, we are able to derive the parameter-free error estimates described as follows, whose proof is omitted for simplicity.

Theorem 5.1. *Let \mathbf{u} be the weak solution of problem (5.1) and \mathbf{u}_h be the solution of problem (5.2), respectively. Then there holds*

$$\|\mathbf{u} - \mathbf{u}_h\|_1 \lesssim h \|\mathbf{f}\|_0.$$

Moreover, if Ω is convex, we have

$$\|\mathbf{u} - \mathbf{u}_h\|_0 \lesssim h^2 \|\mathbf{f}\|_0.$$

Here, the hidden positive constant C is independent of h and λ .

6. Some discussions

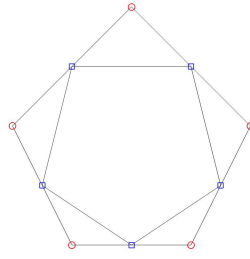


Fig. 2: The second type of mesh refinement. The red circle points denote the original nodes and the blue square points denote the added nodes after once refinement.

It is obvious that the lowest-order conforming virtual element on triangular meshes is exactly the P_1 -conforming finite element. In this case, if the mesh refinement in Fig. 1 is replaced by the one given in Fig. 2, then our method is reduced to the one given by Brenner and Sung in [12].

Our analysis also applies for the mesh assumption given in [13, 16], where each polygon admits a virtual quasi-uniform and regular triangulation:

- A1.** For each $K \in \mathcal{T}_h$, there exists a “virtual triangulation” \mathcal{T}_K of K such that \mathcal{T}_K is uniformly shape regular and quasi-uniform. The corresponding mesh size of \mathcal{T}_K is proportional to h_K . Each edge of K is a side of a certain triangle in \mathcal{T}_K .

Due to the large flexibility of the meshes in VEMs, in this case one can refine the mesh just by taking the midpoint of each edge of K as a new hanging node (see Fig. 3). It’s obvious that the resulting fine mesh denoted by \mathcal{T}_h^* still satisfies the assumption **A1**.

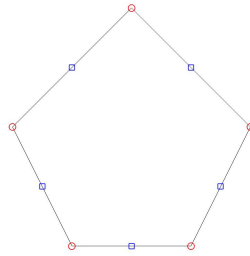


Fig. 3: The third type of mesh refinement. The refined element satisfying the mesh assumption **A1**. The red circle points denote the original nodes, the blue square points denote the added nodes after once refinement.

For meshes under assumption **A1** with refinement way depicted in Fig. 3, it is evident that the construction in Lemma 4.2 or Lemma 5.1 is still valid. Therefore, we can still obtain the locking-free property and the optimal convergence rates in the same manner.

7. Numerical Experiments

In this section, we present some numerical tests for the locking-free conforming VEMs (3.5) and (5.2) to confirm the theoretical results. All the tests are implemented in Matlab R2016a.

Let \mathbf{u} be the exact solution of (2.1) (resp. (5.1)) and \mathbf{u}_h be the discrete solution of the proposed VEM (3.5) (resp. (5.2)). Since the VEM solution \mathbf{u}_h is not explicitly known inside the polygonal elements, as in [9], we will evaluate the computable errors by comparing the exact solution \mathbf{u} with the elliptic projection $\Pi_1^E \mathbf{u}_h$ of \mathbf{u}_h . In this way, the discrete L^2 error ErrL2 and H^1 error ErrH1 are respectively quantified by

$$\text{ErrL2} = \left(\sum_{E \in \mathcal{T}_h^*} \|\mathbf{u} - \Pi_1^E \mathbf{u}_h\|_{0,E}^2 \right)^{1/2} \quad \text{and} \quad \text{ErrH1} = \left(\sum_{E \in \mathcal{T}_h^*} \|\mathbf{u} - \Pi_1^E \mathbf{u}_h\|_{1,E}^2 \right)^{1/2}.$$

7.1. The pure displacement problem

In this test, we consider the linear elasticity problem (2.1) on $\Omega = (0, 1)^2$ with homogeneous Dirichlet boundary conditions. The load term \mathbf{f} is chosen such that the exact solution of (2.1) is

$$\mathbf{u}(x_1, x_2) = \begin{pmatrix} (-1 + \cos(2\pi x_1)) \sin(2\pi x_2) \\ (1 - \cos(2\pi x_2)) \sin(2\pi x_1) \end{pmatrix} + \frac{1}{\mu + \lambda} \sin(\pi x_1) \sin(\pi x_2) \begin{pmatrix} 1 \\ 1 \end{pmatrix}.$$

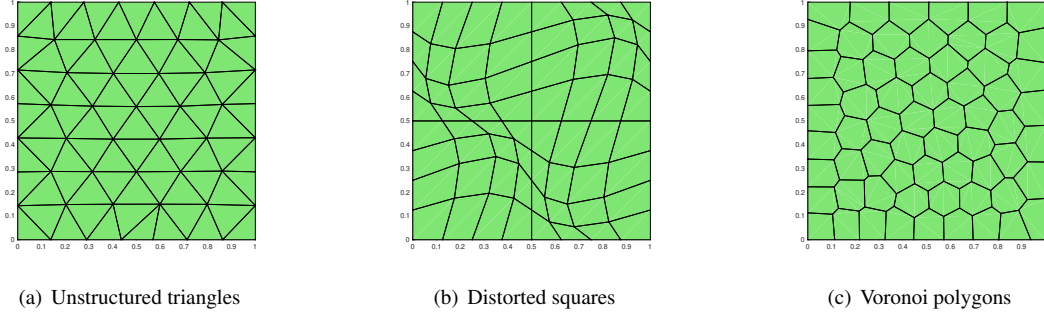


Fig. 4: Three families of meshes.

Case 1: We first consider the locking-free property with respect to different mesh shapes. To do so, we choose three different sequences of meshes, labeled by \mathcal{M}_1 , \mathcal{M}_2 , \mathcal{M}_3 , as shown in Fig. 4, where \mathcal{M}_1 is a sequence of meshes composed of unstructured triangles, \mathcal{M}_2 is a sequence of meshes composed of distorted squares, and \mathcal{M}_3 is a sequence of meshes composed of Voronoi polygons. The distorted meshes are obtained by mapping the position (ξ, ζ) of equal squares meshes through the smooth coordinate transformation

$$x_1 = \xi + \frac{1}{10} \sin(2\pi\xi) \sin(2\pi\zeta), \quad x_2 = \zeta + \frac{1}{10} \sin(2\pi\xi) \sin(2\pi\zeta).$$

And the polygonal meshes are generated by the MATLAB toolbox - PolyMesher introduced in [27]. We only reports the results for the refinement type given in Fig. 2, since the results of the other two types are almost the same, which are omitted.

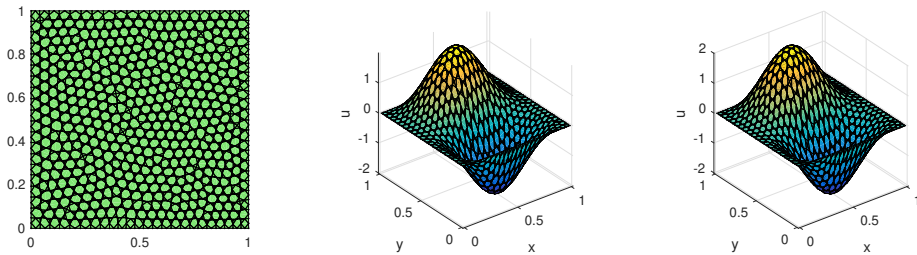


Fig. 5: Numerical and exact solutions for polygonal mesh on \mathcal{M}_3 .

Let $\mu = 1$ and $\lambda = 10^6$. We display the nodal values of the elliptic projection $\Pi_1 \mathbf{u}_h$ on \mathcal{M}_3 in Fig. 5, from which we observe that the numerical solutions are well matched with the exact ones.

The H^1 and L^2 errors computed as functions of mesh size h for the mesh sequences $\{\mathcal{M}_i\}_{i=1}^3$ are depicted in Fig. 6 as a log-log plot. For each fixed pair (λ, μ) , the convergence rate with respect to h is estimated by assuming $\text{Err}(h) = ch^\alpha$ and computing a least squares fit to this log-linear relation. We see that the errors ErrH1 and ErrL2 converge at the optimal rate $O(h^1)$ and $O(h^2)$ respectively, and are not affected by the shape of the mesh discretization. It is worth noting that, the proposed VEM shows a satisfactory stability with respect to the nearly incompressible case ($\lambda = 10^6$).

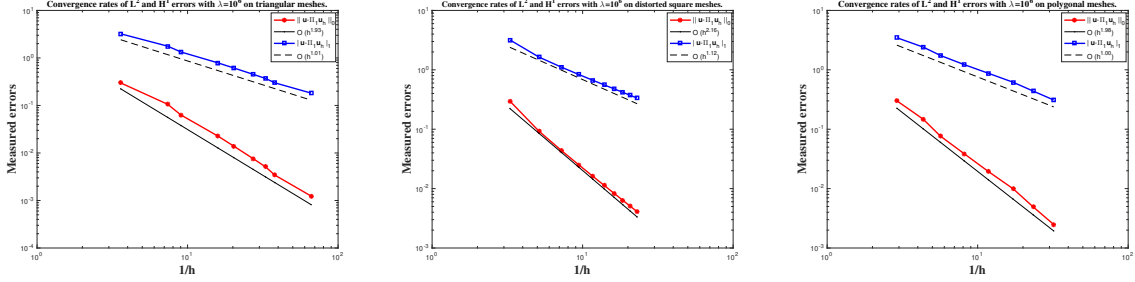


Fig. 6: L^2 and H^1 errors for different sequences of meshes.

Case 2: We further investigate the uniform convergence of the proposed VEM, i.e., the robustness with respect to λ . We consider the Voronoi polygonal meshes \mathcal{M}_3 and choose the original mesh refinement shown in Fig. 1.

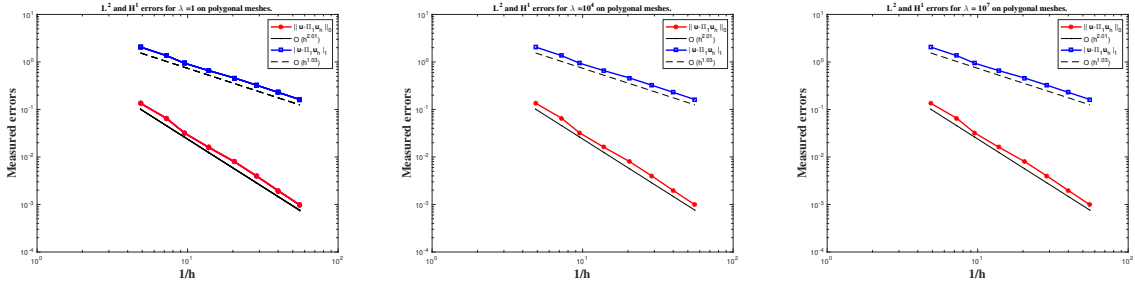


Fig. 7: L^2 and H^1 errors for $\lambda \in \{1, 10^4, 10^7\}$ on meshes \mathcal{M}_3 .

Let $\mu = 1$ and $\lambda \in \{1, 10^4, 10^7\}$. The convergence graphs of the errors ErrH1 and ErrL2 for different values of λ are displayed in Fig. 7. We observe that all the errors are almost the same and the method converges with the optimal rates, which is in agreement with the theoretical predictions in Theorems 4.1 and 4.2. Furthermore, we take $\lambda \in \{10^j, j = 0, 1, \dots, 7\}$ on a fixed mesh in \mathcal{M}_3 with $h = 0.048909$. As shown in Tab. 1, the errors ErrH1 and ErrL2 are hardly affected by the choice of λ , which shows the proposed VEM is locking-free.

Tab. 1: H^1 and L^2 errors with different values of λ on the fixed mesh.

λ	1	10	10^2	10^3	10^4	10^5	10^6	10^7
ErrH1	4.608e-1	4.606e-1	4.612e-1	4.613e-1	4.613e-1	4.613e-1	4.613e-1	4.613e-1
ErrL2	7.912e-3	8.003e-3	8.041e-3	8.046e-3	8.046e-3	8.046e-3	8.046e-3	8.046e-3

7.2. The mixed boundary conditions

In this test, we solve the following linear elasticity problem on $\Omega = (0, 1)^2$ with general boundary conditions:

$$\begin{cases} -\text{div} \sigma(\mathbf{u}) = \mathbf{f} & \text{in } \Omega, \\ \mathbf{u} = \mathbf{g}_1 & \text{on } \Gamma_1, \\ \sigma(\mathbf{u})\mathbf{n} = \mathbf{g}_2 & \text{on } \Gamma_2, \end{cases} \quad (7.1)$$

where, $\Gamma_2 = \{(x_1, x_2) \mid 0 \leq x_1 \leq 1, x_2 = 0\}$ and $\Gamma_1 = \partial\Omega \setminus \Gamma_2$. We select the load term f and the boundary conditions such that the analytical solution of problem (7.1) is

$$u(x_1, x_2) = \begin{pmatrix} \sin(x_1) \sin(x_2) \\ \cos(x_1) \cos(x_2) \end{pmatrix} + \frac{1}{\lambda} \begin{pmatrix} x_1 \\ x_2 \end{pmatrix}.$$

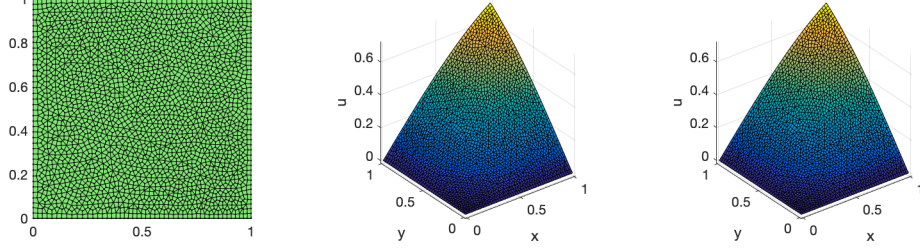


Fig. 8: Numerical and exact solutions for polygonal mesh on \mathcal{M}_3 .

Case 1: We take $\mu = 0.5$ and $\lambda \in \{1, 10^4, 10^7\}$ on Voronoi polygonal meshes \mathcal{M}_3 and choose the original mesh refinement shown in Fig. 1.

The nodal values of the elliptic projection $\Pi_1 u_h$ are shown in Fig. 8. The results of the two errors ErrH1 and ErrL2 versus the mesh size h for different λ are illustrated in Tabs. 2-3. As observed, the optimal rates of convergence are achieved for both cases.

Tab. 2: Convergence rate w.r.t. H^1 norm for $\lambda \in \{1, 10^4, 10^7\}$ on meshes \mathcal{M}_3 .

$\lambda \setminus h$	0.205168	0.137785	0.104895	0.072235	0.048909	0.034884	0.024930	0.017949	Rate
1	4.506e-2	3.023e-2	2.133e-2	1.516e-2	1.050e-2	7.412e-3	5.198e-3	3.673e-3	1.02
10^4	4.506e-2	3.022e-2	2.133e-2	1.516e-2	1.050e-2	7.411e-3	5.197e-3	3.673e-3	1.02
10^7	4.506e-2	3.022e-2	2.133e-2	1.516e-2	1.050e-2	7.411e-3	5.197e-3	3.673e-3	1.02

Tab. 3: Convergence rate w.r.t. L^2 norm for $\lambda \in \{1, 10^4, 10^7\}$ on meshes \mathcal{M}_3 .

$\lambda \setminus h$	0.205168	0.137785	0.104895	0.072235	0.048909	0.034884	0.024930	0.017949	Rate
1	2.233e-3	1.018e-3	4.971e-4	2.528e-4	1.205e-4	5.803e-5	2.934e-5	1.473e-5	2.05
10^4	2.252e-3	1.067e-3	5.168e-4	2.718e-4	1.303e-4	6.078e-5	3.121e-5	1.570e-5	2.03
10^7	2.252e-3	1.067e-3	5.168e-4	2.718e-4	1.303e-4	6.078e-5	3.121e-5	1.570e-5	2.03

Case 2: We fix $\mu = 0.5$ and $\lambda = 10^3$ on Voronoi polygonal meshes \mathcal{M}_3 and choose the three types of mesh refinement way shown in Fig. 1-2. We observed from Fig. 9 that the proposed VEM yields the optimal convergence rates for the two errors, which are uniform with respect to the choices of mesh refinement way.

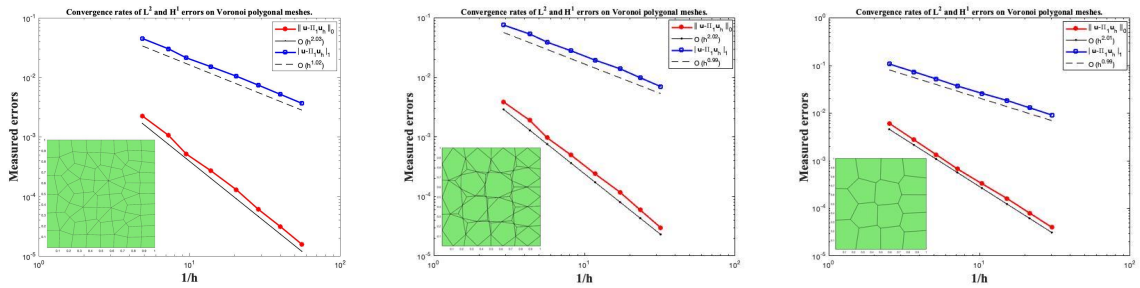


Fig. 9: L^2 and H^1 errors for three types of mesh refinement way on meshes \mathcal{M}_3 in Test 2.

8. Conclusions

We proposed a locking-free conforming VEM in the lowest order case for solving the linear elastic problems, which is an evolution of the locking-free finite element in [12] to general polygonal meshes by using the reduced integration technique. The parameter-free property and the optimal error estimate are established. Numerical results are consistent with theoretical findings.

References

- [1] R. A. Adams and J. J. F. Fournier. *Sobolev Spaces*, volume 140. Second edition, 2003.
- [2] B. Ahmad, A. Alsaedi, F. Brezzi, L. D. Marini, and A. Russo. Equivalent projectors for virtual element methods. *Comput. Math. Appl.*, 66(3):376–391, 2013.
- [3] E. Artioli, S. de Miranda, C. Lovadina, and L. Patruno. A stress/displacement virtual element method for plane elasticity problems. *Comput. Methods Appl. Mech. Engrg.*, 325:155–174, 2017.
- [4] E. Artioli, S. de Miranda, C. Lovadina, and L. Patruno. A family of virtual element methods for plane elasticity problems based on the Hellinger-Reissner principle. *Comput. Methods Appl. Mech. Engrg.*, 340:978–999, 2018.
- [5] L. Beirão da Veiga, F. Brezzi, A. Cangiani, G. Manzini, L. D. Marini, and A. Russo. Basic principles of virtual element methods. *Math. Models Meth. Appl. Sci.*, 23(1):199–214, 2013.
- [6] L. Beirão da Veiga, F. Brezzi, and L. D. Marini. Virtual elements for linear elasticity problems. *SIAM J. Numer. Anal.*, 51(2):794–812, 2013.
- [7] L. Beirão da Veiga, F. Brezzi, L. D. Marini, and A. Russo. The hitchhiker’s guide to the virtual element method. *Math. Models Meth. Appl. Sci.*, 24(8):1541–1573, 2014.
- [8] L. Beirão da Veiga, C. Lovadina, and D. Mora. A virtual element method for elastic and inelastic problems on polytope meshes. *Comput. Methods Appl. Mech. Engrg.*, 295:327–346, 2015.
- [9] L. Beirão da Veiga, C. Lovadina, and A. Russo. Stability analysis for the virtual element method. *Math. Models Methods Appl. Sci.*, 27(13):2557–2594, 2017.
- [10] K. Berbatov, B. S. Lazarov, and A. P. Jivkov. A guide to the finite and virtual element methods for elasticity. *Appl. Numer. Math.*, 169:351–395, 2021.
- [11] S. C. Brenner and L. R. Scott. *The Mathematical Theory of Finite Element Methods*. Springer, New York, 3rd edition, 2008.
- [12] S. C. Brenner and L.-Y. Sung. Linear finite element methods for planar linear elasticity. *Math. Comp.*, 59(200):321–338, 1992.
- [13] F. Brezzi, A. Buffa, and K. Lipnikov. Mimetic finite differences for elliptic problems. *M2AN Math. Model. Numer. Anal.*, 43(2):277–295, 2009.
- [14] E. Cáceres, G. N. Gatica, and F. A. Sequeira. A mixed virtual element method for a pseudostress-based formulation of linear elasticity. *Appl. Numer. Math.*, 135:423–442, 2019.
- [15] A. Cangiani, E. H. Georgoulis, T. Pryer, and O. J. Sutton. A posteriori error estimates for the virtual element method. *Numer. Math.*, 137(4):857–893, 2017.
- [16] L. Chen and J. Huang. Some error analysis on virtual element methods. *Calcolo*, 55(1):Paper No. 5, 23, 2018.
- [17] P. Clément. Approximation by finite element functions using local regularization. *Rev. Française Automat. Informat. Recherche Opérationnelle Sér.*, 9(R-2):77–84, 1975.
- [18] M. Costabel and M. Dauge. On the inequalities of Babuška-Aziz, Friedrichs and Horgan-Payne. *Arch. Ration. Mech. Anal.*, 217(3):873–898, 2015.
- [19] F. Dassi, C. Lovadina, and M. Visinoni. A three-dimensional Hellinger-Reissner virtual element method for linear elasticity problems. *Comput. Methods Appl. Mech. Engrg.*, 364:112910, 17, 2020.
- [20] V. Dhanush and S. Natarajan. Implementation of the virtual element method for coupled thermo-elasticity in Abaqus. *Numer. Algorithms*, 80(3):1037–1058, 2019.
- [21] A. L. Gain, C. Talischi, and G. H. Paulino. On the virtual element method for three-dimensional linear elasticity problems on arbitrary polyhedral meshes. *Comput. Methods Appl. Mech. Engrg.*, 282:132–160, 2014.
- [22] T. J. R. Hughes, M. Cohen, and M. Haroun. Reduced and selective integration techniques in the finite element analysis of plates. *Nuclear Engineering & Design*, 46(1):203–222, 1978.
- [23] D. Y. Kwak and H. Park. Lowest-order virtual element methods for linear elasticity problems, 2021.
- [24] D. S. Malkus and T. J. R. Hughes. Mixed finite element methods — reduced and selective integration techniques: A unification of concepts. *Computer Methods in Applied Mechanics and Engineering*, 1978.
- [25] D. Mora and G. Rivera. A priori and a posteriori error estimates for a virtual element spectral analysis for the elasticity equations. *IMA J. Numer. Anal.*, 40(1):322–357, 2020.
- [26] B. D. Reddy and D. van Huyssteen. A virtual element method for transversely isotropic elasticity. *Comput. Mech.*, 64(4):971–988, 2019.
- [27] C. Talischi, G. H. Paulino, A. Pereira, and I. F. M. Menezes. Polymesher: a general-purpose mesh generator for polygonal elements written in Matlab. *Struct. Multidiscip. Optim.*, 45(3):309–328, 2012.
- [28] X. Tang, Z. Liu, B. Zhang, and M. Feng. A low-order locking-free virtual element for linear elasticity problems. *Comput. Math. Appl.*, 80(5):1260–1274, 2020.
- [29] B. Zhang and M. Feng. Virtual element method for two-dimensional linear elasticity problem in mixed weakly symmetric formulation. *Appl. Math. Comput.*, 328:1–25, 2018.
- [30] B. Zhang, J. Zhao, Y. Yang, and S. Chen. The nonconforming virtual element method for elasticity problems. *J. Comput. Phys.*, 378:394–410, 2019.